

Athermal Broadband Graphene Optical Modulator with 35 GHz Speed

Hamed Dalir,^{†,‡} Yang Xia,^{†,‡} Yuan Wang,[†] and Xiang Zhang^{*,†,‡,⊥}

[†]NSF Nano-scale Science and Engineering Center (NSEC), University of California at Berkeley, 3112 Etcheverry Hall, Berkeley, California 94720, United States

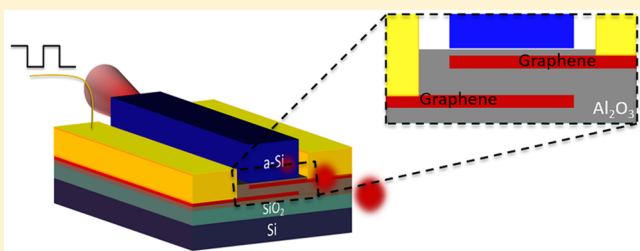
[‡]Material Sciences Division, Lawrence Berkeley National Laboratory, Berkeley, California 94720, United States

[⊥]Department of Physics, King Abdulaziz University, Jeddah, 21589, Saudi Arabia

Supporting Information

ABSTRACT: Optical modulators with ultrahigh speed, small footprint, large bandwidth, robust athermal operation, and complementary metal-oxide semiconductor (CMOS) compatibility are important devices for optical communication and computing applications. Compared to the conventional optical modulators, graphene modulators have attracted great interest due to their large optical bandwidth with an ultracompact footprint. However, their practical applications are limited by the trade-off between speed and optical bandwidth, with a critical issue of temperature tolerance. In this work, we experimentally demonstrate an athermal graphene optical modulator with a 140 nm bandwidth in the entire optical communication regime (1500–1640 nm), with robust high-temperature operation. The device is based on a planar structure with double-layer graphene, leading to the high modulation speed, up to 35 GHz through reduction of the total resistance, and capacitance (9 fF). We observe speed stability in a wide range of temperatures (25–145 °C). The ultracompact footprint (18 μm^2) of the device promises the next generation of on-chip optical interconnections for efficient communication.

KEYWORDS: graphene modulator, broadband, athermal operation, ultrahigh speed, double-layer



To boost the development of future supercomputers and data centers, ideal optical modulators are demanded with ultrahigh speed, small footprint, large optical bandwidth, athermal operation, and complementary metal-oxide semiconductor (CMOS) compatibility. Modulators are classified into two operational categories: electrorefractive and electroabsorptive. For the refractive approach, the modulation is typically achieved by varying the plasma dispersion effect and free carrier absorption in silicon to control the real part of material permittivity. However, for a single-pass two-beam interference like Mach–Zehnder’s, such a change is typically poor. Hence, a device several hundreds of micrometers long must be employed to manipulate the relative phase of the interfering beams for output power control.^{1–3} This results in a large footprint and a high capacitance, which consequently raises the power consumption. Other refractive modulator designs with multiple-pass single-beam interference, such as resonators, require a large quality factor ($>10^4$) or a narrowband modulation (<0.1 nm), which results in a stringent fabrication process. In addition, a precise temperature stabilization to keep the device on resonance is indispensable, causing an increase in the total power consumption.^{4,5} In contrast, absorptive modulators (such as germanium-based devices) utilize the changes of the imaginary part of the material permittivity by applying an electrical field through the structure, mostly with a reverse bias voltage on a p–i–n-like structure.

The electroabsorption effect of germanium has offered a high modulation speed but with a limited optical bandwidth due to finite band gap.^{6,7} As a result it cannot cover the entire optical communication regime (1525–1565 nm (C band) and 1570–1610 nm (L band)). Furthermore, CMOS-compatible applications require special processes (such as epitaxial growth, wafer bonding, or die bonding), which limits the thermal stability of the final devices.^{6–9}

Graphene, a monolayer of carbon atoms formed in a honeycomb lattice, is appealing for optical modulation^{4,10–13} applications due to its unique electrical and optoelectronic properties. Among these are (1) ultrafast modulation speed (several hundreds of GHz), thanks to its high carrier mobility of more than $200\,000\text{ cm}^2/(\text{V}\cdot\text{s})$;^{14–18} (2) broadband operation with a constant absorption of $\pi e^2/\hbar c = 2.293\%$, where \hbar and c are the Plank constant and speed of light in a bulk material, which covers a broad range from visible to infrared wavelengths;^{19,20} (3) CMOS compatibility with the demonstrated wafer-scale integration on silicon in past few years;²¹ and (4) unique temperature stability related to its exceptional thermal conductivity.¹³ With all of these merits,

Received: June 13, 2016

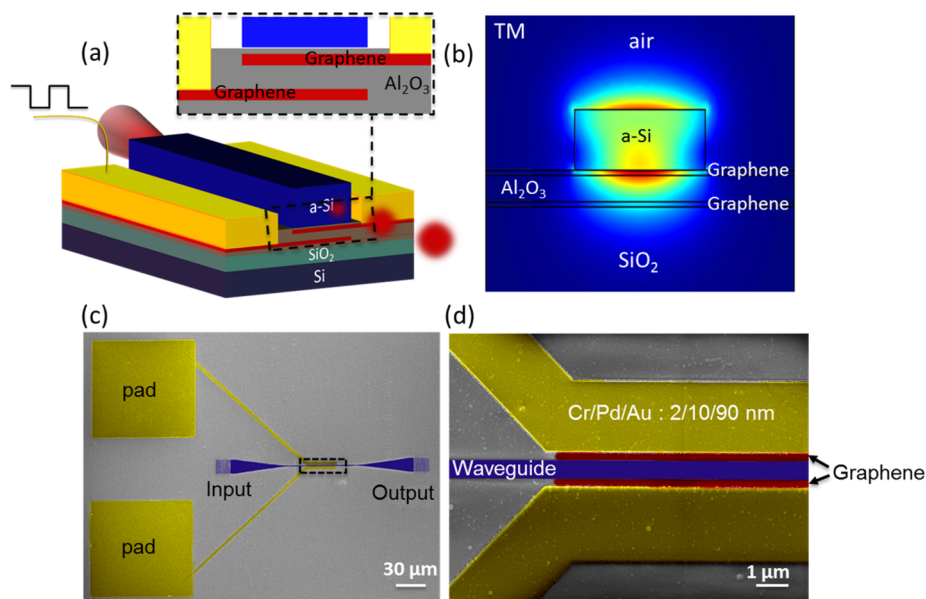


Figure 1. Device design for a high-speed broadband modulator. (a) Cross-section schematic of the device showing two layers of graphene separated by a 120 nm Al_2O_3 dielectric interlayer to form a capacitor. (b) Finite element method (FEM) calculation of the TM mode in the silicon waveguide. Due to the larger overall tangential electric field integration underneath the waveguide, the absorption of the TM mode is as large as $0.1 \text{ dB}/\mu\text{m}$, and a 3 dB modulation depth is expected from the current device geometry. (c) False-color SEM image illustrating the waveguide, input/output couplers, and Cr/Pd/Au metallization. Planar surfaces enable large improvement of material conductivity and contacts by employing the RTA technique and reduction of the capacitance through increasing the interlayer thickness. (d) Zoom-in image of dashed area in (c). Top and bottom graphene layers (red) overlap in the $600 \text{ nm} \times 30 \mu\text{m}$ long waveguide. Gold areas indicate metal contacts.

graphene is expected to be integrated with silicon photonics for the next generation of short-reach optical interconnects.^{15,22}

Here we report the experimental demonstration of a graphene-based electroabsorption modulator with a 35 GHz modulation speed, while absorption is actively controlled by tuning the Fermi level through electrical gating of a graphene double layer. A 2 dB modulation depth within the range of optical communication wavelengths (1500–1640 nm), under ambient conditions, was obtained. More importantly, we show that the modulation performance of our device remains immune to a large range of changes in the temperature (25–145 °C). This is crucial for practical interconnections and communication systems.

EXPERIMENTAL METHODS

To facilitate high-speed and broadband operation, a planar structure is developed by relocating the double-layer graphene underneath the waveguide. This new design allows us to achieve a 10 times thicker spacer layer between the graphene layers compared to the previous work to reduce the device capacitance.¹¹ The contact resistivity has been improved using rapid thermal annealing (RTA). These lead to a more than 1-order enhancement of the modulation speed. In order to fabricate the double-layer graphene optical modulator, wet thermal oxidation and atomic layer deposition (ALD) were employed to form a $1 \mu\text{m}$ silica and a 20 nm thick Al_2O_3 , respectively, which prevents the leakage of the optical mode into the silicon substrate. Next, chip-sized graphene grown on copper was transferred to the goal substrate by employing the wet transfer method²³ (Figure S1a). The electrode and a contact pad for the bottom graphene layer were defined by e-beam and UV lithography, respectively, followed by e-beam evaporation of Cr/Pd/Au with a thickness of 2/10/90 nm (Figure S1b). During the RTA process, the sample was ramped

in 30 s to 300 °C and stabilized at 300 °C for about 1 min with a flowing gas of 10% hydrogen in nitrogen into the chamber, with a repetition cycle of five times. The graphene is patterned by e-beam lithography. Oxygen plasma was used to remove the undesired graphene region (Figure S1c). It is noted that a pristine graphene with the hydrophobic nature of the basal plane encounters the difficulty in direct deposition of high dielectric constant material through the ALD method. Therefore, a seeding layer of 2-nm-thick Al_2O_3 was deposited onto the bottom graphene by e-beam evaporation. The planar design of graphene layers lets us form an interlayer of 120-nm-thick Al_2O_3 with ALD for ultrafast optoelectronic uses (Figure S1d). The top graphene layer was then transferred, forming a capacitor structure (Figure S1f). Similar procedures to those for the bottom graphene layer were performed to allow the active tuning of graphene layers (Figure S1f–h). The Raman spectroscopy data indicate good-quality graphene for both top and bottom layers (Figure S2). A layer of 270-nm-thick, amorphous silicon (a-Si) was deposited by PECVD (Figure S1i). Eventually a $600 \text{ nm} \times 30 \mu\text{m}$ (width \times length) silicon waveguide, with both ends connected to a pair of grating couplers (period = 870 nm, optimized for transverse magnetic (TM) mode with $\lambda = 1550 \text{ nm}$) was fabricated via e-beam lithography and transformer coupled plasma (TCP) etching (Figure S1j). We carried out a two-dimensional finite element method (FEM) simulation using COMSOL Multiphysics. The calculation results indicate that the absorption of the TM mode ($0.1 \text{ dB}/\mu\text{m}$) is greater than the transverse electric (TE) mode due to its better overlap with graphene, and a 3 dB modulation depth is expected from the current device geometry shown in Figure 1b. Figure 1c and d show the false-color SEM image including the waveguide, input/output couplers, and Cr/Pd/Au metallization. Top and bottom graphene layers (red colors) overlap well with the modulator waveguide.

MEASUREMENT RESULTS

To study the dynamic response of the double-layer graphene modulator, an unmodulated RF signal with -7 dBm from the calibrated Anritsu 37397D vector network analyzer (VNA) was combined with a bias direct current (dc) voltage of 25 V through an SHF BT-110 bias-tee and applied between the bottom and top layers of graphene. The coaxial cable was connected to the device with a GGB model 40A-GS microwave probe. Losses from the cabling, bias-tee, and probe were subtracted. A distribute feedback (DFB) laser at 1550 nm was used to externally generate the light into the modulator. The radiofrequency (RF)-modulated signal was then transferred to the VNA via the BPDV3120R u^2t photodiode cascaded with a UA1L65VM broadband postamplifier. We measured small-signal RF (S_{21} : ratio between the optical amplitude modulation and the RF signal). Figure 2 illustrates the S_{21} results, while a

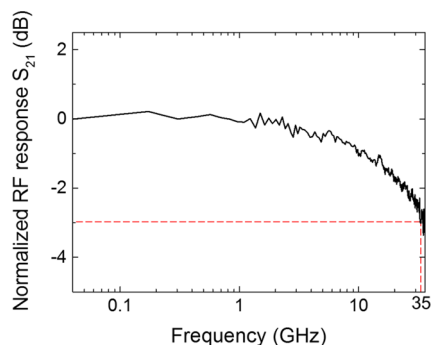


Figure 2. Radio frequency response of the device. The 3 dB cut-off frequency of 35 GHz was obtained with an RF power of -7 dBm biased at $V_{DC} = 25$ V. Speed performance is limited by device RC time constant. An estimation of the geometric capacitance of the measured device is 9 fF, while our measurement indicates that a high series resistance ($\sim 500 \Omega$) mainly arises from the contact resistance between the graphene layer and metal electrode, limiting the current speed performance.

bandwidth of 35 GHz limited by the RC time constant of our fabricated modulator is obtained. The RC is restricted by the dimension of the capacitor, graphene sheet resistance, and contact resistance. An estimation of the measured device's geometric capacitance is 9 fF, while our measurement revealed that the high series resistance ($\sim 500 \Omega$) mainly came from the contact resistance between the graphene layer and palladium electrode (pad), which is the key issue for the current speed limitation. Using the state-of-the-art process, the series resistance of the device can be considerably reduced to below 50 ohm,^{4,24} which combined with a microstrip electrode design terminated with a matched impedance²⁵ can significantly increase the speed of the modulator.

Typically, interference-based silicon devices such as resonators or Mach–Zehnders are highly sensitive to high-temperature operation due to the large thermo-optic coefficient effect in silicon. To study the temperature dependence of the operating characteristics, we tested the 30- μm -long waveguide modulator throughout a large temperature range of 25–145 °C. We studied the slope of the RF response (S_{21}) at 1550 nm throughout a large temperature range of 25–145 °C (raw data plotted in Figure S3). As shown in Figure 3, the slope virtually remains unchanged as the temperature rises, which denotes a robust speed performance. In addition, a 1.9 dB modulation depth at a high temperature of 145 °C with the same swing

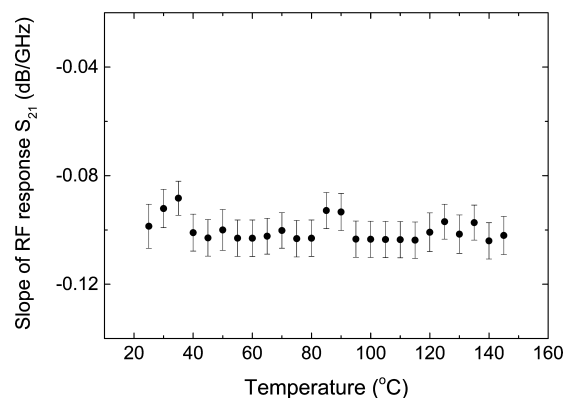


Figure 3. Robust athermal operation of the graphene modulator under a large temperature range. The slope of the RF response S_{21} under different temperatures remains virtually the same. At a high temperature of 145 °C a modulation depth of 1.9 dB is obtained, indicating a robust athermal operation of the device, which is a key factor for practical approaches.

voltage was obtained, indicating less dependency on the temperature change. The robust athermal operation in modulators is critical to optoelectronic interconnection and communication systems for ultrafast efficient modulation.

The static results on the transmission of the graphene waveguide modulator with various bias voltages were measured at the standard communication wavelength of 1550 nm (Figure 4a). While most of the transmission loss comes from the two grating couplers (-13.5 dB for both couplers), the minimum transmission of the waveguide is -16.4 dB, at which 2 dB modulation depth with TM mode excitation was obtained for a 30- μm -long waveguide modulator. An extremely low insertion loss of -0.9 dB was measured by comparing the output of two identical waveguides with and without graphene layers. Applying a voltage swing of 25 V to the modulator is required to turn the modulator from the OFF to ON state and vice versa, which corresponds to a power consumption of 1.4 pJ/bit.

The absorption of graphene is adjusted by the electrical gating. The band structure of graphene is composed of two bands that are degenerate at the so-called Dirac points. Due to the nature of the monolayer (low density of states), the position of the Fermi level can be modified readily by changing the accumulation charge. Considering an undoped monolayer graphene (Figure 4 region II), the Fermi level is at the Dirac point. Under the illumination of photons with an energy of $\hbar\nu$ (where \hbar and ν are the Planck and light frequency, respectively), the transmission would be attenuated. However, when the graphene sheet is either hole- or electron-doped (Figure 4 regions I and III), its Fermi level drops or rises, respectively. When the charging is sufficient to raise (or drop) the Fermi level by the photon's half energy above (or below) the Dirac point, the interband transition is considerably suppressed, and hence higher transmission is allowed. In our device, when a positive voltage is applied to the top layer (bottom layer is effectively negatively biased), a less positive voltage is needed to suppress the absorption compared with the negative voltage case. This is because the absorption is mainly from the top layer graphene, which is closer to the waveguide mode, and that layer is initially p-doped. We examined the optical bandwidth of our double-layer graphene device in a large range of optical communication wavelengths. A uniform modulation depth under different optical wavelengths (1500–1640 nm) was

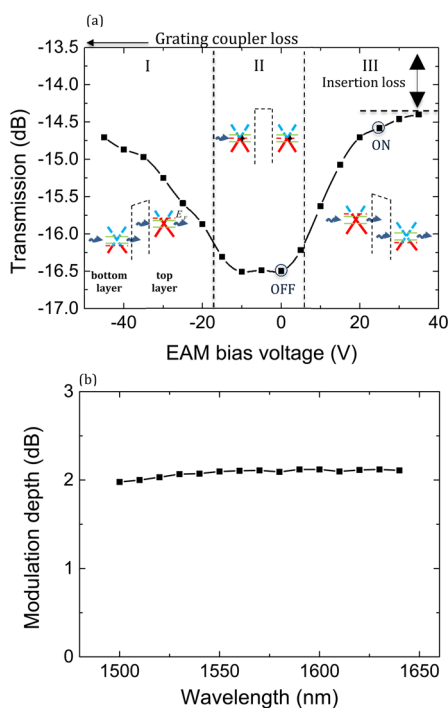


Figure 4. Broadband functionality of the planar modulator. (a) Static result of a planar double-layer graphene modulator. A modulation depth of ~ 2 dB is achieved on a $30 \mu\text{m}$ long device with a swing voltage of 25 V at the standard optical wavelength of $1.55 \mu\text{m}$. (Inset) Band profiles of graphene (blue and red for unoccupied and occupied states, respectively) for regions I, II, and III, in which the arrows represent the incident and transmitted photons. (b) Uniform modulation depth of the device across the full measured wavelength range from 1500 to 1640 nm covering the entire optical communication region (1525–1565 nm (C band) and 1570–1610 nm (L band)) has been observed with a fixed swing voltage. Such a broadband functionality in a modulator is important to boost the capacity of optical short-reach interconnects.

observed with a constant swing voltage (Figure 4b). Such a broadband functionality in a modulator is important to boost the capacity of optical short-reach interconnects. A comparison of performances between our modulator and established modulation techniques is provided in Table S1.

CONCLUSION

In conclusion, we have experimentally demonstrated a planar double-layer graphene modulator with an ultrafast operation up to 35 GHz. A uniform modulation depth of 2 dB for the entire optical communication wavelengths (1500–1640 nm) was obtained with an ultracompact footprint of $18 \mu\text{m}^2$. Robust athermal operation of the modulator with no noticeable change in speed performance of the device at a high temperature up to 145°C was presented, critical for the next generation of optical communication and computing.

ASSOCIATED CONTENT

Supporting Information

The Supporting Information is available free of charge on the ACS Publications website at DOI: 10.1021/acsphtons.6b00398.

Additional information (PDF)

AUTHOR INFORMATION

Corresponding Author

*E-mail (X. Zhang): xiang@berkeley.edu.

Author Contributions

#H. Dalir and Y. Xia contributed equally to this work.

Notes

The authors declare no competing financial interest.

ACKNOWLEDGMENTS

The experiment of this research was supported by the Office of Naval Research (ONR) MURI program under Grant No. N00014-13-1-0678; the simulation was supported by the ‘Light-Material Interactions in Energy Conversion’ Energy Frontier Research Center funded by the U.S. Department of Energy, Office of Science, Office of Basic Energy Sciences under Award Number DE-AC02-05CH11231.

REFERENCES

- (1) Soref, R. A.; Bennett, B. R. Electrooptical effects in silicon. *IEEE J. Quantum Electron.* **1987**, *23*, 123–129.
- (2) Lee, M.; Katz, H. E.; Erben, C.; Gill, D. M.; Gopalan, P.; Heber, J. D.; McGee, D. J. Broadband modulation of light by using an electro-optic polymer. *Science* **2002**, *298* (5597), 1401–1403.
- (3) Alloati, L.; Palmer, R.; Diebold, S.; Pahl, K. P.; Chen, B.; Dinu, R.; Fournier, M.; Fedeli, J. M.; Zwick, T.; Freude, W.; Koos, C.; Leuthold, J. 100 GHz silicon-organic hybrid modulator. *Light: Sci. Appl.* **2014**, *3*, e173.
- (4) Phare, C. T.; Daniel Lee, Y.-H.; Cardenas, J.; Lipson, M. Graphene electro-optic modulator with 30 GHz bandwidth. *Nat. Photonics* **2015**, *9*, 511–514.
- (5) Guarino, A.; Poberaj, G.; Rezzonico, D.; Deglincocenti, R.; Gunter, P. Electro-optically tunable microring resonators in lithium niobate. *Nat. Photonics* **2007**, *1*, 407–410.
- (6) Chaisakul, P.; Marris-Morini, D.; Frigerio, J.; Chrastina, D.; Rouified, M. S.; Cecchi, S.; Crozat, P.; Isella, G.; Vivien, L. Integrated germanium optical interconnects on silicon substrates. *Nat. Photonics* **2014**, *8*, 482–488.
- (7) Kuo, Y. H.; Lee, Y. K.; Ge, Y. S.; Ren, S.; Roth, J. E.; Kamins, T. I.; Miller, D. A. B.; Harris, J. Strong quantum-confined Stark effect in germanium quantum-well structures on silicon. *Nature* **2005**, *437* (7063), 1334–1336.
- (8) Liang, D.; Bowers, J. E. Recent progress in lasers on silicon. *Nat. Photonics* **2010**, *4* (8), 511–517.
- (9) Kekatpure, R. D.; Lentine, A. The suitability of SiGe multiple quantum well modulators for short reach DWDM optical interconnects. *Opt. Express* **2013**, *21*, 5318–5331.
- (10) Liu, M.; Yin, X. B.; Zhang, X. Double-layer graphene optical modulator. *Nano Lett.* **2012**, *3*, 1482–1485.
- (11) Liu, M.; Yin, X.; Ulin-Avila, E.; Geng, B.; Zentgraf, T.; Ju, L.; Wang, F.; Zhang, X. A graphene-based broadband optical modulator. *Nature* **2011**, *474*, 64–67.
- (12) Li, W.; Chen, B.; Meng, C.; Fang, W.; Xiao, Y.; Li, X.; Hu, Z.; Xu, Y.; Tong, L.; Wang, H.; Liu, W.; Bao, J.; Shen, Y. R. Ultrafast all-optical graphene modulator. *Nano Lett.* **2014**, *14*, 955–959.
- (13) Hu, Y. T.; Pantouvaki, M.; Brems, S.; Asselberghs, I.; Huyghebaert, C.; Geisler, M.; Alessandri, C.; Baets, R.; Absil, P.; Van Thourhout, D.; Van Campenhout, J. Broadband 10 Gb/s operation of graphene electro-absorption modulator on silicon. *Laser Photon. Rev.* **2016**, *10* (2), 307–316.
- (14) Gan, X.; Shiue, R.-J.; Gao, Y.; Meric, I.; Heinz, T. F.; Shepard, K.; Hone, J.; Assefa, S.; Englund, D. Chip-integrated ultrafast graphene photodetector with high responsivity. *Nat. Photonics* **2013**, *7*, 883–887.
- (15) Kim, K.; Choi, J. Y.; Kim, T.; Cho, S. H.; Chung, H. J. A role for graphene in silicon-based semiconductor devices. *Nature* **2011**, *479*, 338–344.

- (16) Bolotin, K. I.; Sikes, K. J.; Jiang, Z.; Klima, M.; Fudenberg, G.; Hone, J.; Kim, P.; Stormer, H. L. Ultrahigh electron mobility in suspended graphene. *Solid State Commun.* **2008**, *146*, 351–355.
- (17) Koppens, F. H. L.; Chang, D. E.; de Abajo, F. J. G. Graphene plasmonics: a platform for strong light-matter interactions. *Nano Lett.* **2011**, *11*, 3370–3377.
- (18) Hong, X.; Posadas, A.; Zou, K.; Ahn, C. H.; Zhu, J. High-Mobility Few-Layer Graphene Field Effect Transistors Fabricated on Epitaxial Ferroelectric Gate Oxides. *Phys. Rev. Lett.* **2009**, *102*, 136808.
- (19) Nair, R. R.; Blake, P.; Grigorenko, A. N.; Novoselov, K. S.; Booth, T. J.; Stauber, T.; Peres, N. M. R.; Geim, A. K. Fine Structure Constant Defines Visual Transparency of Graphene. *Science* **2008**, *320* (5881), 1308–1308.
- (20) Mak, K. F.; Sfeir, M. Y.; Wu, Y.; Lui, C. H.; Misewich, J. A.; Heinz, T. F. Measurement of the optical conductivity of graphene. *Phys. Rev. Lett.* **2008**, *101*, 196405.
- (21) Bae, S.; Kim, H.; Lee, Y.; Xu, X.; Park, J. S.; Zheng, Y.; Balakrishnan, J.; Lei, T.; Kim, H. R.; Song, Y. I.; Kim, Y. J.; Kim, K. S.; Özyilmaz, B.; Ahn, J. H.; Hong, B. H.; Iijima, S. Roll-to-roll production of 30-in. graphene films for transparent electrodes. *Nat. Nanotechnol.* **2010**, *5*, 574–578.
- (22) Bhimanapati, G. R.; Lin, Z.; Meunier, V.; Jung, Y.; Cha, J. J.; Das, S.; Xiao, D.; Son, Y.; Strano, M. S.; Cooper, V. R.; Liang, L.; Louie, S. G.; Ringe, E.; Zhou, W.; Kim, S. S.; Naik, R. R.; Sumpter, B. G.; Terrones, H.; Xia, F.; Wang, Y.; Zhu, J.; Akinwande, D.; Alem, N.; Schuller, J. A.; Schaak, R. E.; Terrones, M.; Robinson, J. A. Recent Advances in Two Dimensional Materials Beyond Graphene. *ACS Nano* **2015**, *9*, 11509.
- (23) Suk, J. W.; Kitt, A.; Magnuson, C. W.; Hao, Y. F.; Ahmed, S.; An, J. H.; Swan, A. K.; Goldberg, B. B.; Ruoff, R. S. Transfer of CVD-grown monolayer graphene onto arbitrary substrates. *ACS Nano* **2011**, *5* (9), 6916–6924.
- (24) Leong, W. S.; Gong, H.; Thong, J. T. L. Low-contact-resistance graphene devices with nickel-etched-graphene contacts. *ACS Nano* **2014**, *8* (1), 994–1001.
- (25) Lee, M.; Katz, H. E.; Erben, C.; Gill, D. M.; Gopalan, P.; Heber, J. D.; McGee, D. J. Broadband Modulation of Light by Using an Electro-Optic Polymer. *Science* **2002**, *298* (5597), 1401–1403.